Pergamon

PII: S0191–8141(98)00008–X

Journal of Structural Geology, Vol. 20, No. 6, pp. 707 to 726, 1998

0191-8141/98 $19.00 + 0.00

Volume loss and metasomatism during cleavage formation in carbonate rocks

SCOT G. DAVIDSON*, DAVID J. ANASTASIO, GRAY E. BEBOUT, JAMES E. HOLL† and CHRISTOPHER A. HEDLUND‡

Department of Earth and Environmental Services, Lehigh University, Bethlehem, PA 18015-3188, U.S.A.

(*Received* 13 *January* 1997; *accepted in revised form* 23 *January* 1998)

Abstract—Controversy exists regarding the amount of volume loss associated with cleavage development. A combination of geometrical and geochemical techniques provides evidence for contemporaneous passive concentration (volume loss) and metasomatism leading to the formation of cleavage in carbonate lithologies and emphasizes the relationship between observational scales and textural heterogeneity. Comparison of protoliths and weakly- to strongly-cleaved rocks along steep, layer-parallel strain gradients within the Doublespring duplex, Lost River Range, Idaho enables quantitative assessments of geometric transformation and elemental mass transfer accompanying progressive deformation. Geometric finite strain analysis documents shortening in the Z direction at low strains ($\bar{\varepsilon}_s < 0.15$) and in both the Z and Y directions at higher strains ($\bar{\varepsilon}_s > 0.15$). Unbalanced shortening in Z and Y with extension in X results in volume loss. Geometrically derived volume strain estimates at the 1–4 cm^3 scale indicate volumetric dilations of from −2% to −12% in uncleaved to weakly-cleaved rocks, and from −20% to −50% in strongly- to very strongly-cleaved rocks. Small-scale significant volume losses and gains contrast with the estimated volume loss of $< 3\%$ associated with duplex formation at the 100 km^3–1 km^3 scale due to the localization of strain within thin deformation zones.

Sampling scale is also a factor in evaluating the major and trace element and O and C isotope compositions of the variably deformed rocks. Samples collected at the 4–15 cm^3 scale reflect mixtures of chemically and mineralogically distinct selvage and microlithon domains. Microdrilling of samples at scales of a few cubic millimeters to 1 cm^3 affords examination of chemical and isotopic differences among individual selvages and microlithons. The data for microdrilled samples demonstrate depletion of Ca and ^{18}O and enrichment of K, Al, Si, Ti, Fe, Na, Mg and P in selvages relative to microlithons and nearby undeformed carbonate layers. The enrichments of some elements (Mg, P, Na and possibly Fe) are more compatible with a passive concentration mechanism, whereas the concentrations of other elements, particularly K, Al, Si and Ti, require significant metasomatic addition during deformation. Shifts in O-isotope compositions of deformed samples relative to the protolith $\delta^{18}O$ values unequivocally demonstrate open-system behavior during deformation. Trends of deformed samples toward lower $\delta^{18}O$ with increasing strain and the $\delta^{18}O$ values of veins are compatible with infiltration by H_2O-rich fluids with relatively low $\delta^{18}O_{V\text{-}SMOW}$ (near 0‰).

The formation of disjunctive cleavage at the Doublespring duplex occurred by passive concentration resulting from calcite dissolution and related volume loss, and neo-crystallization of illite + kaolinite + quartz ± anatase in selvages as a result of metasomatic additions. Chemical and geometric strain softening within selvages likely led to enhanced and preferential fluid flow in selvages.

INTRODUCTION

Cleavage in low-grade sedimentary rocks is a domainal tectonic fabric consisting of less deformed microlithons, often resembling the protolith, and more deformed selvage zones. Selvages are generally fine-grained and optically opaque and may be smooth to serrated, or straight to anastomosing. They are often regarded as 'insoluble residues' or 'carbon films' and in carbonate rocks, are commonly attributed to passive concentration accompanying calcite dissolution (Alvarez *et al.*, 1976, 1978; Engelder and Marshak, 1985). Textures such as sutured grain boundaries and truncated fossils record dissolution, whereas fibrous overgrowths record precipitation during diffusive mass transfer, the mechanism largely accepted as being responsible for disjunctive cleavage in sandstones (Nickelsen, 1972; Geiser, 1974; Gray, 1978), limestones (Nickelsen, 1972; Groshong, 1975; Alvarez *et al.*, 1978), and dolostones (Schweitzer and Simpson, 1986). Dissolution planes and fibrous overgrowths define finite strain axes ($X > Y > Z$ principal axes of the finite strain ellipsoid) and document transgranular mass transfer related to cleavage formation. During deformation, volume changes may occur depending upon the degree of open vs closed system behavior. Inferred magnitudes of chemical change, however, appear to be dependent upon scales of observation. Alvarez *et al.* (1978) and Engelder and Marshak (1985) concluded that the passive concentration of insoluble residual material is responsible for cleavage formation in argillaceous limestones during closed system behavior as a result of relatively localized mass transfer. Wintsch *et al.* (1991) and Lee *et al.* (1986) suggested that limited

*Current address: Dames & Moore, Willow Grove, PA 19090, U.S.A.
†Current address: Exxon Production Research Co., Houston, TX 77252-2189, U.S.A.
‡Current address: Shell Exploration and Production Technology Co., Houston, TX 77001-0481, U.S.A.

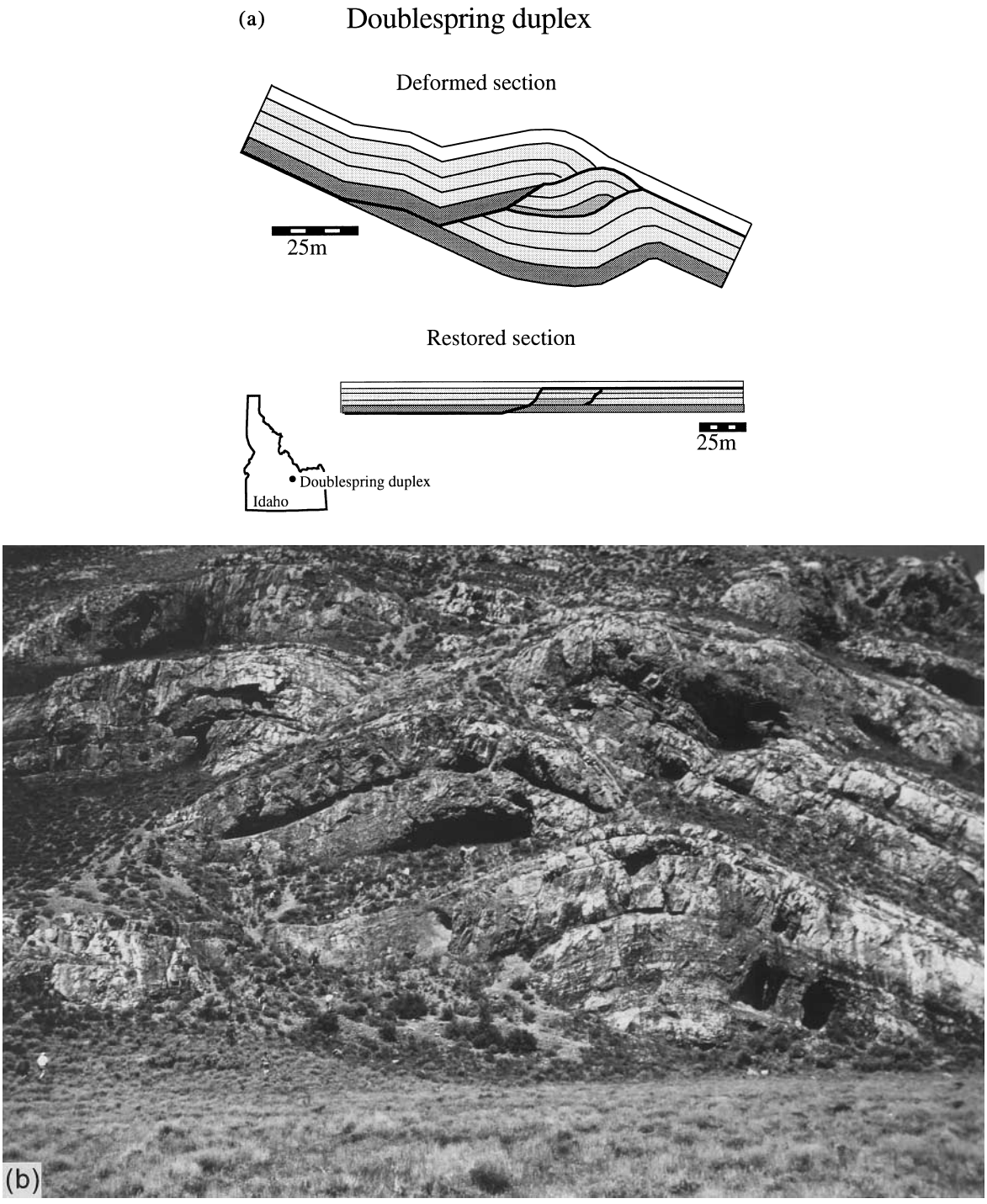

Fig. 1. (a) Bed-length and area balanced deformed- and restored-state cross-sections of Doublespring duplex. Restored section at half-scale. Adapted from Hedlund *et al.* (1994) and Davidson (1996). (b) Photograph of Doublespring duplex towards 340° showing upper, middle and lower folds and roof thrust. Field of view is ~75 m in the horizontal direction.

open-system conditions involving metasomatic processes and external additions may also be an important component of cleavage development in slates at a scale of a few centimeters.

Previous attempts to assess volume strains have yielded contradictory results. For example, geometrical determinations of volume strains using deformed reduction spots, graptolites, and/or conodonts show volume losses of 20–60% within Welsh and Appalachian slates (Ramsay and Wood, 1973; Beutner and Charles, 1985; Wright and Henderson, 1992; Bailey *et al.*, 1994; Goldstein, 1995). Geochemical studies of similar lithologies, however, document little or no net volume loss associated with cleavage formation (Erslev and Mann, 1984; Erslev and Ward, 1994; Srivastava *et al.*, 1995). The conflicting results of these two approaches are likely related to uncertainties and assumptions inherent in these research methodologies

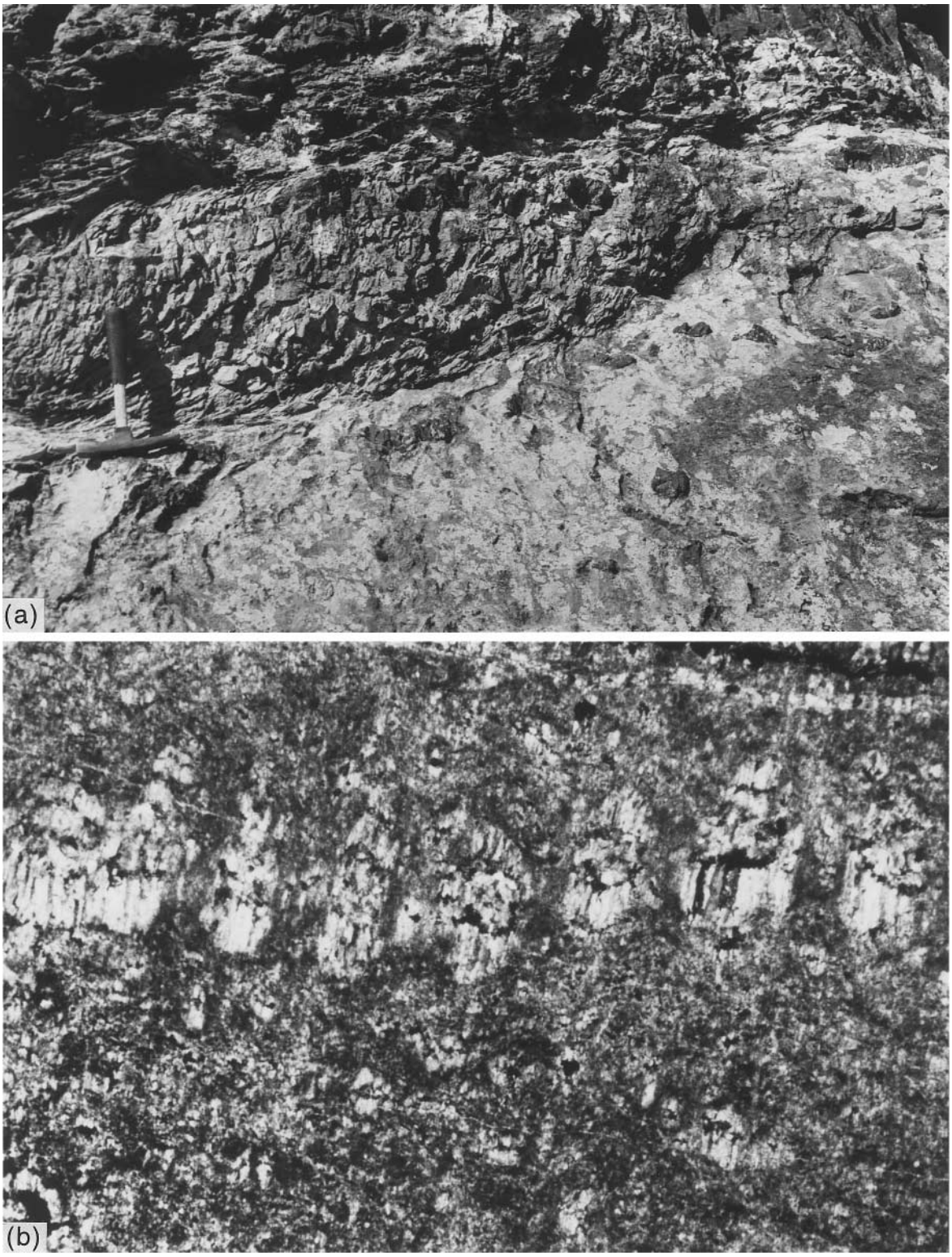

Fig. 2. Meso- to microscopic textures indicative of mass transfer. (a) Deformation zone on southwestern limb of lower fold. Chert nodules trace bedding from the weakly cleaved area on the right side of the photograph through the strongly cleaved zone on the left. Note layer parallel calcite veins. Field of view is ~5 m wide. See Fig. 3(b) for sketch and sample distribution. (b) Photomicrograph of a portion of sample 94-L-129 illustrating quartz-replaced bioclasts with straight, antitaxial, fibrous calcite overgrowths, truncated and sutured bioclast grain boundaries, and microveins. XY section with X vertical, parallel to strain fringe fibers and orthogonal to the trace of microveins. Field of view ~4.5 mm wide.

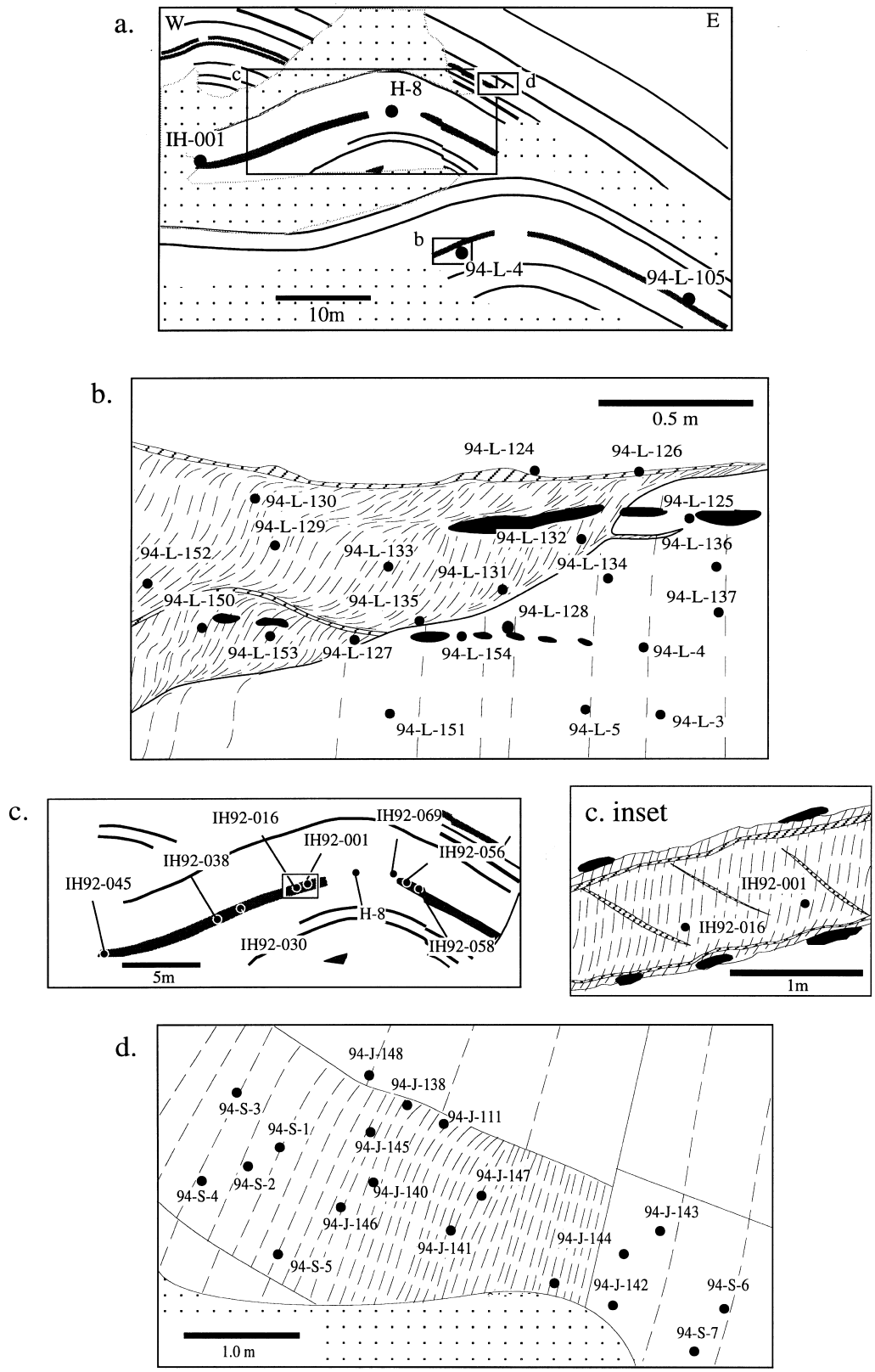

Fig. 3. Sample localities. (a) Sketch of Doublespring duplex showing location of protolith samples. Broad, dark lines represent shear zones, thin lines are bedding traces, stipples are areas covered in field. Dashed, boxed areas (b), (c), and (d) show sampling locations of lower fold, middle fold, and roof thrust zone, respectively. Filled circles represent protolith sampling locations with corresponding sample number. In (b), (c), and (d) dotted lines show cleavage spacing and orientation in outcrop view.

and to natural lithologic and deformation heterogeneity. Geometric techniques rely on assessments of the three-dimensional rock strain at relevant scales and knowledge of the sedimentary fabrics and strain partitioning. Geochemical approaches ideally require undeformed protoliths to constrain initial elemental and stable isotopic composition. Protolith constraints of these types are not always available, therefore, some studies have relied on hypothetical protolith compositions and/or have assumed the immobility of elements such as Al, Ti or Zr (e.g. Ague, 1991, 1994). Other studies have used stable isotope compositions to determine degrees of open- and closed-system behavior during deformation, integrating the isotopic work with detailed field and petrographic observations regarding the nature and relative timing of host-rock deformation and vein formation (e.g. Kerrich, 1986; Rye and Bradbury, 1988; Gray *et al*., 1991; Kirschner *et al*., 1995).

The purpose of this study was to examine the scale and mechanisms of mass transfer and volume strain related to cleavage formation in carbonate lithologies within the Doublespring duplex, Lost River Range, Idaho. The structure is near a Sevier-aged cleavage front, enabling a gradation in cleavage intensities to be examined. The cleavage in the outcrop is controlled by structural position, with steep, local strain gradients occurring between strongly-cleaved fold limbs and uncleaved hinge zones along continuous layers. We exploited the protolith constraints and the range of cleavage intensities using integrated geometrical and geochemical approaches. Three-dimensional finite strain measurements constrain the magnitude and orientation of shape changes and volumetric dilations. Whole-rock and microdrilled major and trace element compositions were used to constrain chemical and mineralogical evolution, while oxygen isotope compositions of calcite in veins and variably deformed rocks allowed assessment of the degrees of open- and closed-system behavior during deformation.

Regional geology

The Lost River Range lies east of the Antler deformation front and north of the Snake River Plain in east-central Idaho. The range consists of a remnant of the Sevier fold and thrust belt which has been exposed by Tertiary–Neogene uplift and extension. The range is a broad synclinorium containing Paleozoic outer-shelf stratigraphy including: (1) a late Paleozoic platform of shallow water clastics and carbonates deposited on a west-facing shelf, (2) distal flysch derived from the Antler highlands forming an eastward-tapering wedge which serves as a décollement within the Hawley thrust sheet and (3) an upper Paleozoic, westerly prograded carbonate platform which contains fault-related folds including the Doublespring duplex. For the Doublespring exposure, peak deformation temperatures of ~220°C were obtained by illite crystallinity (Hedlund *et al*., 1994); regional stratigraphic reconstructions, balanced and restored cross sections of the Idaho–Wyoming–Montana thrust belt, and geobarometry around the Idaho batholith and the Pioneer Metamorphic core complex suggest that compressional deformation within the upper Paleozoic carbonates of the Lost River Range occurred at a depth of ~10 km (Silverberg, 1990; Anastasio *et al*., 1997).

The Doublespring duplex

The Doublespring duplex (Fig. 1) is a hinterland-dipping duplex structure located east of Christian Gulch in the northern Lost River Range, Idaho (Hedlund *et al*., 1994). The duplex consists of a central horse and three anticlinal folds, referred to here as the upper, middle, and lower folds. Each fold exhibits parallel and cylindrical fault-bend fold geometries, curved hinges with interlimb angles ranging from 130° to 145°, and shallow bed cutoff angles. Fold axes for the lower and middle folds converge northward at 10°. In a kinematic study of the Doublespring duplex, Hedlund *et al*. (1994) showed that folds were formed by buckling accommodated by flexural flow in widely spaced (15 m), narrow (0.5–1 m) deformation zones toward pinned hinges, then translated along faults for a minimum shortening of 50 m (38%) towards 070°. The duplex shortens the Scott Peak Formation, which consists of marine biopackstone and sparse biomicritic limestone interbedded with chert-nodule-rich layers. A distinct feature of the duplex is the presence of highly-cleaved, recessed deformation zones located within the limbs of each fold but not within the hinge regions of the folds. A high-strain zone is also present along the roof thrust above the middle fold (Davidson *et al*. 1996). The lower and middle folds repeat a section of several thick beds. The roof thrust zone consists of beds ~10 m higher in the section.

Observation of mass transfer and cleavage

Textural features indicative of mass transfer occur at a variety of scales within the duplex. At the outcrop scale (hundreds of m^3), beds in the core of the middle fold are thickened by 80% relative to the same layers on the hinterland limb of the horse (Fig. 1b). At smaller scales, layer-parallel calcite veins 8–10 cm wide and chert nodules with calcite overgrowths 0.5–2 cm wide vary in distribution over hundreds to tens of cm^3, respectively. Petrographic observations using light and cathodoluminescence microscopy of thin sections cut parallel to cleavage (XY) and perpendicular to the cleavage-bedding intersection (XZ) reveal mass transfer at scales ranging from tens of μm^3 to a few cm^3 (Fig. 2). These microscopic textures include truncated bioclasts (some of which include antitaxial or syntaxial fibrous overgrowths in strain fringes), transgranular

Table 1. Results from strain analysis including Fry and R_f/Φ derived axial strain ratios, principal stretch (1 + extension) values, amount of strain values ($\bar{\varepsilon}_s$), and maximum, minimum, and best estimates of volume strain (ΔV). Errors for values given as $\pm 1\sigma$

Sample	Cleavage intensity	R_{xz} (Fry)	R_{xz} (R_f/Φ)	R_{xy} (Fry)	R_{xy} (R_f/Φ)	$1 + e_x$	$1 + e_y$	$1 + e_z$	$\bar{\varepsilon}_s$	ΔV (min)	ΔV	ΔV (max)
Lower Fold												
94-L-127	very strong		1.8 ± 0.1		1.6 ± 0.1	1.16 ± 0.12	0.73	0.64	0.44	−38	−46	−52
94-L-129	strong	1.8 ± 0.3	1.8 ± 0.1		1.7 ± 0.1	1.30 ± 0.13	0.76	0.63	0.53	−18	−38	−36
94-L-133	strong	1.9 ± 0.1	1.8 ± 0.1		1.6 ± 0.1	1.23 ± 0.12	0.77	0.68	0.45	−26	−36	−43
94-L-135	very strong	2.0 ± 0.1	1.8 ± 0.1		1.5 ± 0.1	1.15 ± 0.12	0.77	0.64	0.43	−35	−43	−50
IH92-157	strong	1.8 ± 0.1										
IH92-069	strong	1.6 ± 0.1	1.6 ± 0.1									
IH92-070	strong	1.9 ± 0.1										
94-L-3	weak		1.2 ± 0.1	1.2 ± 0.1	1.1 ± 0.1	1.05 ± 0.10	1	0.88	0.13	6	−8	−26
94-L-4	weak		1.2 ± 0.1		1.1 ± 0.1	1.04 ± 0.10	1	0.87	0.03	3	−9	−29
94-L-128	weak		1.5 ± 0.1		1.3 ± 0.1	1.20 ± 0.12	0.92	0.8	0.29	4	−12	−24
94-L-136		1.3 ± 0.1			1.1 ± 0.1	1.13 ± 0.11	1	0.87	0.06	21	−2	−14
IH92-118	weak	1.4 ± 0.1										
IH92-119	weak	1.4 ± 0.1										
Mesoscale												
Net/s. limb	strong	1.9 ± 0.2										
Net/s. limb	weak	1.2 ± 0.2										
Middle Fold												
IH92-001	very strong	2.0 ± 0.4	2.0 ± 0.1		1.8 ± 0.1	1.20 ± 0.12	0.7	0.6	0.51	−46	−50	−57
IH92-016	strong	1.5 ± 0.1	1.7 ± 0.2									
IH92-030	strong	2.4 ± 0.1			2.0 ± 0.1							
IH92-038	strong	1.9 ± 0.1			2.1 ± 0.2							
IH92-045	moderate		1.4 ± 0.1		1.2 ± 0.2	1.15 ± 0.12	0.96	0.82	0.24	18	−9	−28
IH92-056	strong	1.5 ± 0.2										
IH92-058	strong		1.4 ± 0.1		1.2 ± 0.1	1.10 ± 0.11	0.92	0.79	0.25	−6	−20	−32
IH92-069	weak	1.6 ± 0.1	1.6 ± 0.1									
IH92-118		2.0 ± 0.1	1.4 ± 0.1									
IH92-119		1.9 ± 0.1	1.6 ± 0.2									
IH92-169		1.9 ± 0.1	1.7 ± 0.1									
DS-93-8	weak	1.1 ± 0.1										
Roof thrust												
94-J-146	strong	1.7 ± 0.1	1.4 ± 0.1	1.2 ± 0.1	1.5 ± 0.1	1.04 ± 0.10	0.7	0.74	0.26	−37	−47	−53
94-J-149	moderate	1.3 ± 0.1	1.3 ± 0.1	1.3 ± 0.1	1.4 ± 0.1							
94-S-1	strong	2.0 ± 0.1	1.6 ± 0.1	1.4 ± 0.1	1.1 ± 0.1	1.04 ± 0.10	0.99	0.65	0.3	−20	−33	−43
	moderate						0.72	0.77	0.27	−30	−41	−48
94-S-2	strong	1.1 ± 0.1	1.4 ± 0.1	1.1 ± 0.1	1.5 ± 0.1	1.08 ± 0.11						
94-S-3	moderate	1.5 ± 0.1	1.4 ± 0.1	1.5 ± 0.1	1.3 ± 0.1	1.02 ± 0.10	0.78	0.76	0.22	−29	−40	−49
94-S-4	moderate	1.2 ± 0.1	1.5 ± 0.1	1.1 ± 0.1	1.2 ± 0.1	1.04 ± 0.10	0.85	0.71	0.23	−25	−37	−46
94-S-5	strong	2.0 ± 0.1	1.4 ± 0.1	1.4 ± 0.1	1.3 ± 0.1	1.04 ± 0.10	0.83	0.77	0.2	−21	−34	−43

cleavage selvages, and a smaller number of orthogonal veins which are evenly spaced every few mm up to a few cm in some samples.

Cleavage is irregularly distributed in the deformed layers at the outcrop. We examined the cleavage fabric in detail within three areas of the duplex (Fig. 3a). One suite of samples was collected from the southwest limb of the lower fold where cleavage transects bedding, which can be traced using chert nodules, across a steep strain gradient from areas with no- or weakly-cleaved rocks to strongly- to very strongly-cleaved rocks within ~2 m along several layers (Figs 2a & 3b). Protolith comparisons were taken from uncleaved rocks adjacent to cleaved rocks within the same stratigraphic layer (Fig. 3a–b). Similar ranges of cleavage intensity, from weakly- to very strongly-cleaved rocks, are present in the middle fold shear zone (Fig. 3c). In this area, the deformation zone is bedding-parallel and located within the limbs of the fold, while the hinge of the fold was pinned during deformation (Hedlund *et al.*, 1994). Protolith samples used to constrain the changes in whole-rock geochemistry, and for geometrical comparison between undeformed and deformed rocks, were collected from this hinge. The third area of sampling is located in a roof thrust zone above the middle fold (Fig. 3d). The roof thrust suite of samples exhibits a gradation in cleavage intensity from moderate to very strong with spacing of 1–5 cm and < 0.5 cm, respectively, over a distance of ~2.5 m. Orientation of the cleavage in all of the sampled zones varies from roughly layer-perpendicular in the interior of the shear zones where cleavage is generally straight, to nearly bedding-parallel where anastomosing cleavage approaches the massive layer-shear zone contact (Fig. 3a–d).

METHODS AND RESULTS

Geometrical analysis

Three-dimensional shape changes associated with cleavage development are based on samples collected along each strain gradient (Table 1). At a scale of 2 m^2, finite bulk strain estimates were made using a reference grid to determine chert nodule distribution

within a non- to weakly-cleaved massive layer and a strongly- to very strongly-cleaved deformation zone of the lower fold (Fig. 4). Two-dimensional finite strain determinations (R_{xz}) using normalized Fry analysis (Erslev, 1988) are $R_{xz} = 1.2 \pm 0.2$ (1σ) and $R_{xz} = 1.9 \pm 0.2$ (1σ) within the massive layer and deformation zone, respectively (Table 1). Errors for mesoscopic finite strain measurements were estimated by randomly analyzing 25 objects subsets of each data set of $n \geq 45$.

Bulk and object finite strain measurements were made at scales of tens of μm^2 to 1–2 cm^2 in principal plane thin sections utilizing normalized Fry analysis in biopackstones and R_f/Φ analysis in sparse biomicrite samples. Strain was determined in multiple areas of individual thin sections, sampled over areas ranging from 1–2 cm^2 to assess heterogeneity, and then averaged to constrain errors of finite strain measurement. Results from micro-scale finite strain determinations ranged from a low of $X{:}Y{:}Z = 1.04 \pm 0.1{:}1.0{:}0.87 \pm 0.1$ ($\bar{\varepsilon}_s = 0.03$) in a weakly-cleaved rock, to a maximum of $X{:}Y{:}Z = 1.2 \pm 0.1{:}0.7 \pm 0.1{:}0.6 \pm 0.1$ ($\bar{\varepsilon}_s = 0.53$) in strongly-cleaved rock (Table 1). The amount of strain:

$$\bar{\varepsilon}_s = (1/\sqrt{3})[(\varepsilon_x - \varepsilon_y)^2 + (\varepsilon_y - \varepsilon_z)^2 + (\varepsilon_z - \varepsilon_x)^2]^{1/2} \quad (1)$$

where

$$\varepsilon_{x,y,z} = \ln(1 + e_{x,y,z}) \quad (2)$$

(Nadai, 1963) provides a useful means of characterizing the magnitude of the finite strain and represents the strain on the octahedral planes (oriented at 45° to the principle planes) of the strain ellipsoid. Lode's parameter [$v = (2\varepsilon_y - \varepsilon_x - \varepsilon_z)/(\varepsilon_x - \varepsilon_z)$] is used to characterize the shape of the strain ellipsoid, oblate or prolate, based upon the relative magnitudes of the principal extensions within the Doublespring samples. A Nadai plot (Hossack, 1968) of v vs $\bar{\varepsilon}_s$ (Fig. 5) indicates an oblate shape at low strains which becomes prolate as strain increases.

Principal extension values ($e_{x,y,z}$ = change in length divided by initial length) were estimated from fibrous overgrowths and micro-veins in XY and XZ planes examined both optically and using cathodoluminescence (Fig. 6). Measurements included three separate linear transects oriented parallel to the trace of cleavage in XZ sections or dip of cleavage in XY sections, over which lengths of tectonic precipitated material

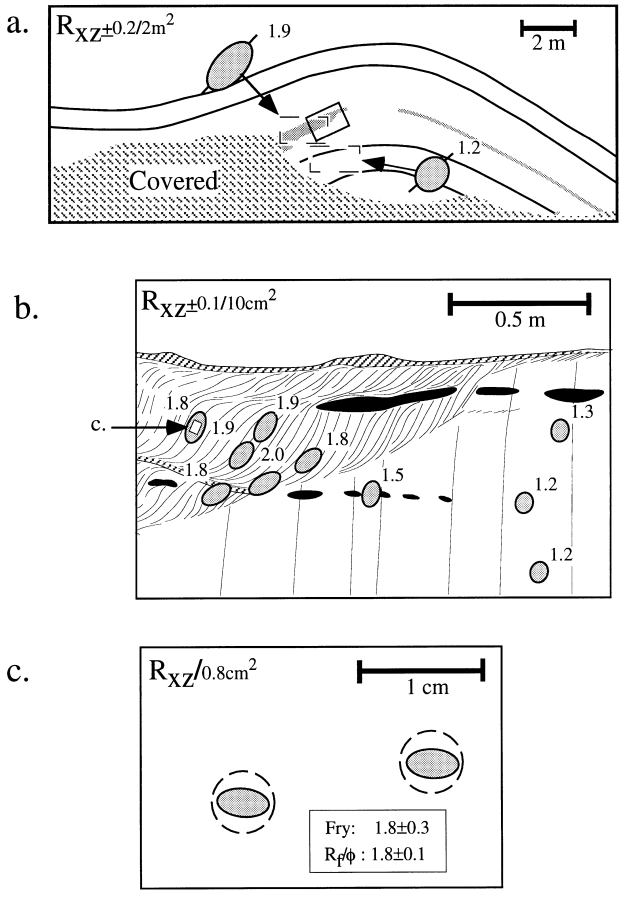

Fig. 4. (a) Ellipses representing the magnitude and orientation of mesoscopic (~4 m^2) finite strain in cleaved and uncleaved areas (dashed rectangles) of the lower fold. (b) Strain ellipses representing microscopic results (~1–4 cm^2) along lower fold strain gradient. (c) Comparison of microscopic normalized Fry and R_f/Φ analysis illustrating thin section scale homogeneity of axial ratio magnitude and orientation. Dashed circle represents area of measurement.

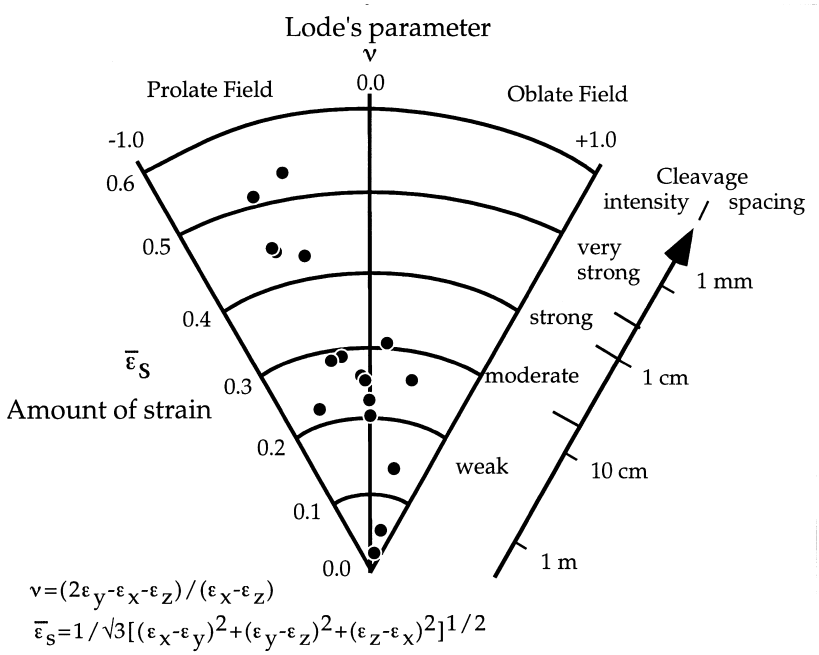

Fig. 5. Plot of Lode's Parameter (v) and amount of strain ($\bar{\varepsilon}_s$) from weakly cleaved samples with low $\bar{\varepsilon}_s$ to strongly cleaved samples with high $\bar{\varepsilon}_s$. Note the transition from oblate field to prolate field as the strain ellipsoid changes shape with degree of deformation. Cleavage intensity and selvage spacing refers to terminology of Alvarez *et al.* (1978).

(veins and overgrowths) were recorded within overlapping windows 0.8 mm in length (Fig. 6c). Using these data sets, absolute extension values were determined and range from $e_x = 0.04$ to 0.30 (Table 1). Errors associated with measurements of principal extension values were determined by averaging values from three individual transects for each sample and are listed in Table 1.

Geometric volume strain determinations were made by calibrating relative finite strain axial ratios in principal planes parallel to cleavage (R_{xz}) and perpendicular to the cleavage-bedding intersection (R_{xy}), with direct measurements of principal extension (e_x) from syntectonic overgrowths and micro-veins. Determinations of $R_{xy} = (1 + e_x)/(1 + e_y)$, $R_{xz} = (1 + e_x)/(1 + e_z)$, and e_x allow the calculation of the proportional volumetric dilation which is given by:

$$1 + \Delta V = (1 + e_x)(1 + e_y)(1 + e_z) \quad (3)$$

(Ramsay and Huber, 1983). Finite strain values (R_{xy} and R_{xz}) used in calculations were based primarily on R_f/Φ analysis in the sparse biomicrites. Volume strain estimates based upon these results ranged from $\Delta V = -2\%$ to -12% in rocks with no- to weak cleavage, to $\Delta V = -20\%$ to -50% in rocks having strong to very strong cleavage (Fig. 7, Table 1). Maximum dilatancy estimates for individual samples, based upon estimates derived using minimum and maximum axial ratio and principal extension values range from $\Delta V = +21\%$ to -26% in rocks with no- to weak-cleavage, to $\Delta V = -6\%$ to -52% in rocks having strong to very strong cleavage. A consideration of the errors associated with dilatancy estimates (Fig. 7) illustrates that, while weakly cleaved rocks may be nearly volume constant, strongly cleaved rocks have lost significant volume at a scale of a few cm^3.

Geochemical analysis

Whole-rock analyses of undeformed and deformed rock samples allowed characterization of mineralogy and chemical and isotopic compositions at the scale of 4–15 cm^3. Microsampling techniques were also utilized in some cases where a few mm^3 were sampled using 1 or 2 mm drill bits. In all cases, the hand specimens used for geochemical analysis were those used for geometrical analysis; these samples represent the least to the most deformed rocks within the three respective sampling zones. Varying combinations of X-ray fluorescence (XRF) and X-ray diffraction (XRD) techniques, carbon–hydrogen–nitrogen (CHN) analyses, O and C isotope analyses, and scanning electron microscopy (SEM) and electron dispersive spectrometry (EDS) techniques were applied to study these samples.

Conventional X-ray fluorescence analyses (by X-ray Assay Laboratories Ltd., Don Mills, Ont., Canada and Activation Laboratories, Ancaster, Ont., Canada, using standard techniques) and X-ray diffraction analyses (at Lehigh University on a Philips APD-3720 automated X-ray diffractometer) were performed on whole-rock samples ranging from the least deformed

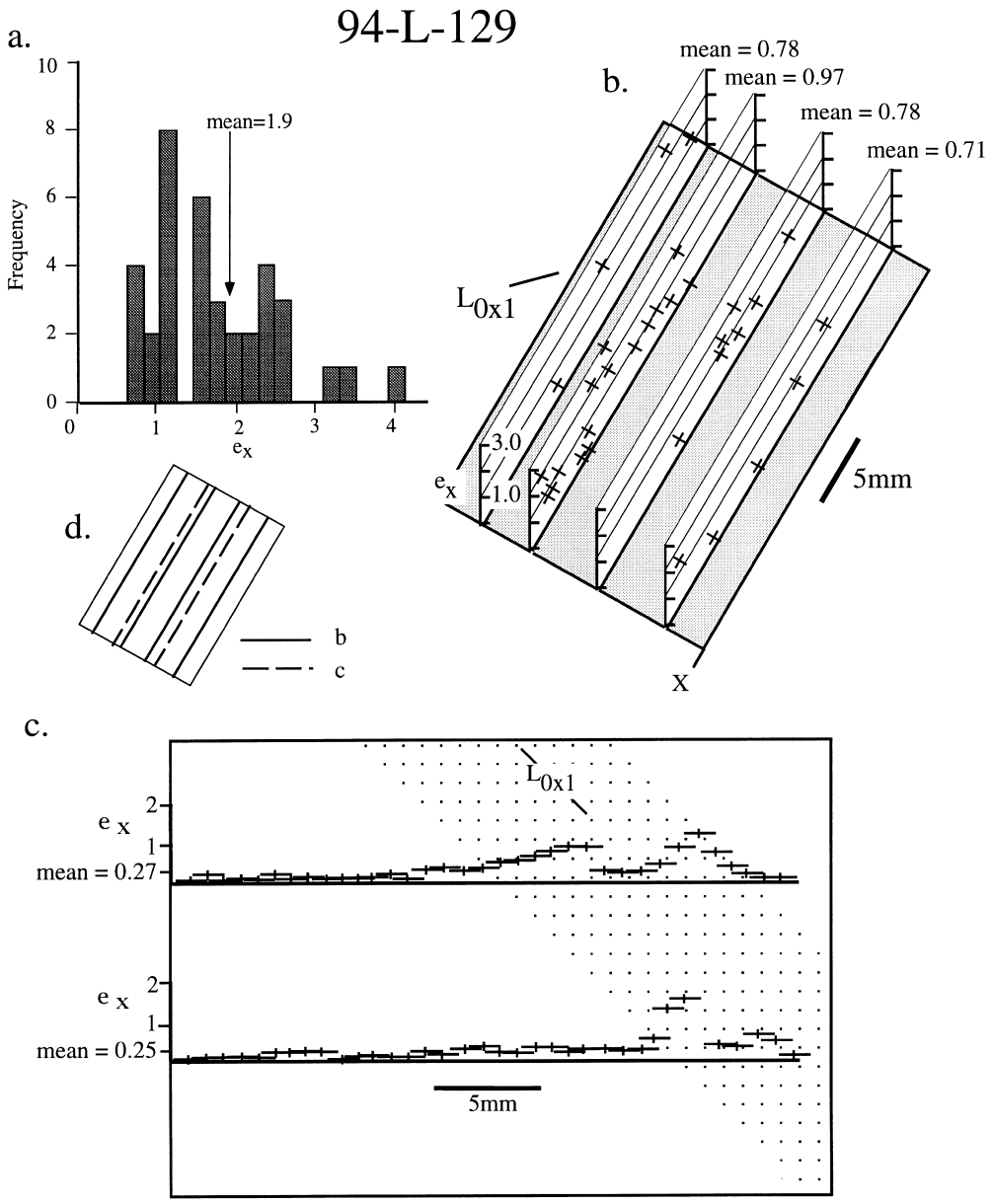

Fig. 6. Assessment of various methods of measuring extension applied to sample 94-L-129. (a) Histogram of extension values derived using individual strain fringes. (b) Measurement of extension averaging the sum of strain fringe extensions over ~2 cm transects. (c) Illustration showing method of measure principal extension using overlapping-windows 0.8 mm in length. Here, cm-scale homogeneous domains of extension can be quantified. See text for further discussion.

to the most deformed and on microsampled cleavage selvage and microlithon domains. The whole-rock XRF major element compositions (data for middle and lower folds in Figs 8 & 9, respectively) demonstrate significant, in some cases strongly correlated (particularly for the middle fold samples, Fig. 8), enrichments in K, Al, Si, Ti, Fe, Mg and P in deformed zones relative to undeformed zones. Calcium concentrations (Figs 8d & 9d) show a corresponding decrease in deformed zones relative to inferred protoliths, showing an overall range in CaO concentration of ~35–54 wt%. The very strongly and pervasively cleaved deformation zone in the middle fold shows more dramatic element co-enrichments compared with the whole-rock samples from the lower fold. For example, there is <2.0 wt% Al_2O_3 in the lower-fold whole-rock samples (Fig. 9) compared with the up to 3.15 wt% Al_2O_3 in the more deformed middle-fold samples (Fig. 8). For the lower fold, major element compositions of samples with little macroscopic to microscopic evidence of deformation highly overlap the compositions of nearby samples judged in the field and petrographically as being more highly deformed (see data for deformed and undeformed whole-rock samples in Fig. 9). In the middle fold, an abrupt, layer-parallel strain gradient exists between a nearly undeformed hinge area and very strongly deformed limbs. This allows hinge samples and samples showing

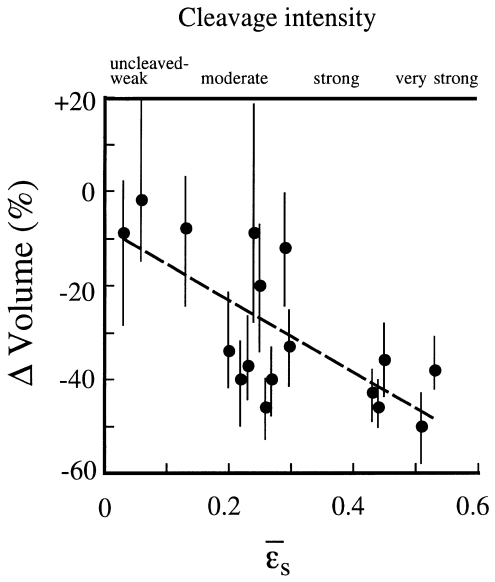

Fig. 7. Geometrically determined dilatency at 3–4 cm^3 scale with individually calculated errors vs $\bar{\varepsilon}_s$ and cleavage intensity. Least-squares, linear regression also shown.

varying degrees of cleavage development to be more clearly distinguished in the field, in thin section, and geochemically (see the more distinct compositions of massive, undeformed layers and variably deformed zones in Fig. 8). For the middle fold, samples of weakly-cleaved rocks have compositions intermediate between those of undeformed (protolith) samples and those of more strongly-cleaved samples.

Major element compositions of microdrilled selvage and microlithon materials and nearby undeformed protoliths better afford chemical characterization of these distinct domains (data for lower fold in Fig. 9). For most elements considered in Fig. 9 (other than Ca), microdrilled materials from nearby undeformed rocks (data for 'Protoliths' in Fig. 9) have concentrations in these elements lower than those of most whole-rock uncleaved samples. Microdrilled individual selvages have higher concentrations in these elements than those of most whole-rock cleaved samples. These observations are consistent with the compositions of the whole-rock samples having resulted from varying mixtures of cleavage selvage and microlithon domains (Fig. 9), even in samples which in hand specimen appear uncleaved. Concentrations of the co-enriched elements in selvages microdrilled from the lower fold are as high as (or higher than) the concentrations of these elements in more pervasively and more highly deformed whole-rock samples in the middle fold. For example, selvages in lower fold samples contain up to 4.3 wt% Al_2O_3, compared with the maximum of 3.15 wt% Al_2O_3 in the strongly deformed whole-rock samples from the middle fold. Overall, the major element geochemical data in Figs 8 and 9 are consistent with greater cleavage development having been accompanied by greater degrees of element enrichment (on a whole-rock basis) in samples from the middle fold deformation zone relative to samples from the same deformed stratigraphic layer in the lower fold.

The concentrations and co-enrichments of K_2O, Al_2O_3, SiO_2 and TiO_2 in selvage samples are consistent with an ~2 illite:1 kaolinite clay mixture, together with varying amounts of quartz and a Ti-oxide (Davidson, 1996). Enrichment in Ba in many selvage samples relative to lower-Al_2O_3, undeformed samples (up to 315 ppm in selvages, compared with concentrations of <65 ppm in undeformed whole-rock samples and microlithons) likely reflects the residence of Ba in illite in the more deformed zones. Mineralogy of the selvages was investigated by XRD with preparation of samples according to methods of Hein *et al.* (1975) and Drever (1973). XRD patterns for selvage materials (with carbonate removed by dissolution) corroborate the dominantly illite and kaolinite mineralogy inferred geochemically. The XRD patterns also indicate the presence of varying amounts of quartz and anatase in selvages.

Fine-scale textures were examined at magnification of up to 1500X using SEM imaging in conjunction with EDS analyses (JOEL 6300F SEM, Link thin-window X-ray detector, Lehigh University). Selvages were found to have increased concentrations of K, Al and Si relative to adjacent microlithons; this observation is consistent with the XRF data presented in Fig. 9(a,c). Platy K–Si–Al-rich grains, interpreted as phyllosilicates, within microlithons have basal planes which are mainly oriented parallel to cleavage (XY) planes. These grains occur in small concentrations along framework grain sutures which resemble microselvages at a scale of a few μms. Within selvages, cleavage-parallel platy grains occur in greater concentration than in microlithons along with abundant neo-crystallized calcite. Phyllosilicate grain size is similar in both microlithons and selvages.

Selvage material was analyzed for the presence of organic carbon using an elemental CHN analyzer (Carlo Erba model 1106, Lehigh University), as cleavage in carbonates is sometimes identified as a 'carbonaceous film' (e.g. De Paor *et al.*, 1991). Removal of the calcite component prior to analysis was done by treating selvage material within a 5N HCL solution. Results from these analyses show that little (0.026 wt%) of the selvage domains at the Doublespring duplex consists of organic carbon.

The stable isotope compositions of C and O of undeformed and deformed whole rocks, veins, and microsampled materials were measured for samples collected along the strain gradients. Analyses were performed on both the whole-rock samples and the microdrilled samples used for the XRF analyses. The use of microdrill sampling techniques allowed the identification of differences in the isotopic compositions of individual microlithon and selvage domains and veins (Figs 10 & 11). Oxygen and C isotope analyses were

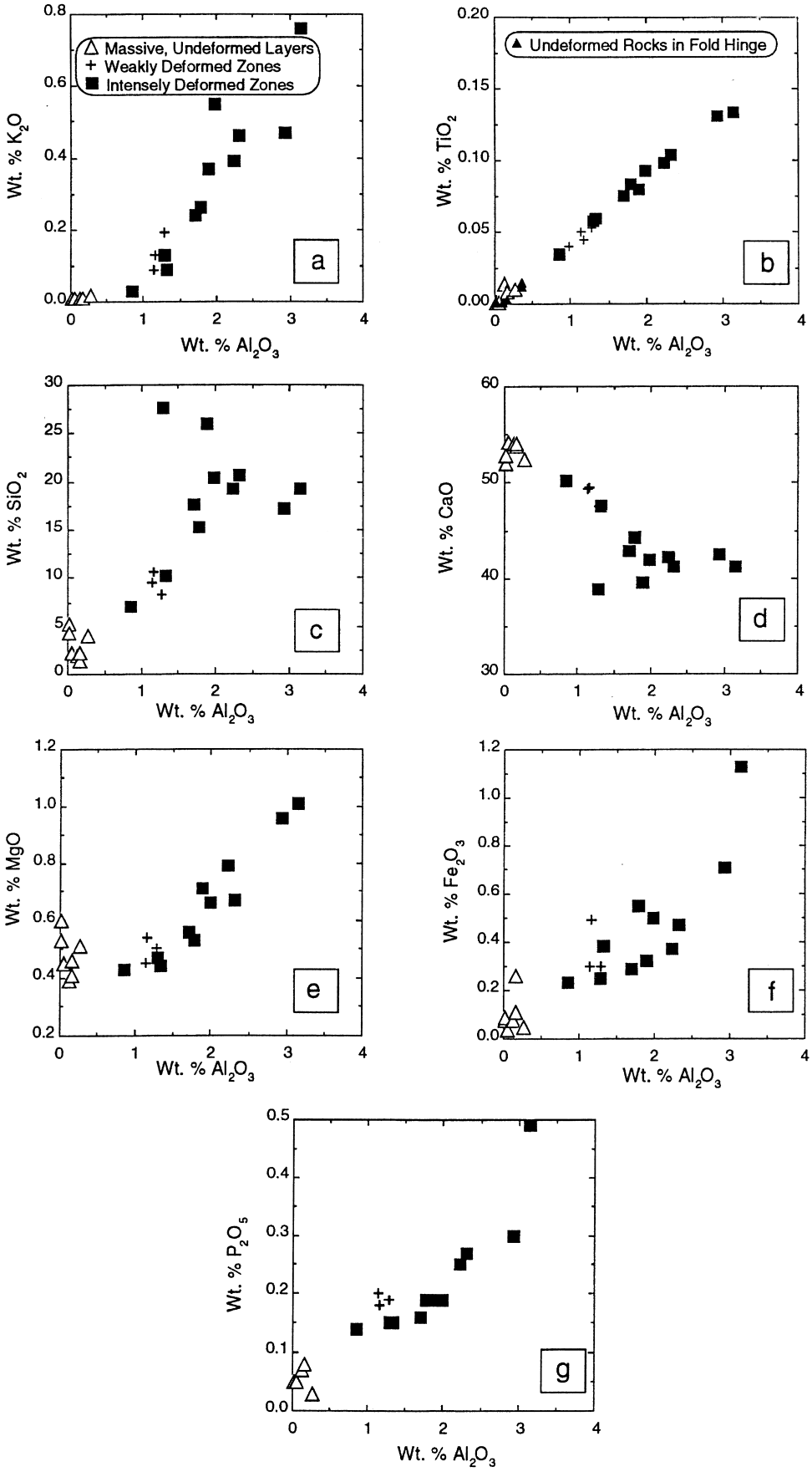

Fig. 8. (a–g) Major element whole-rock data for samples from the middle fold. Symbols used in all figures are defined in (a); in addition, TiO_2 and Al_2O_3 data for samples of undeformed hinge rocks are shown in (b) as solid triangles.

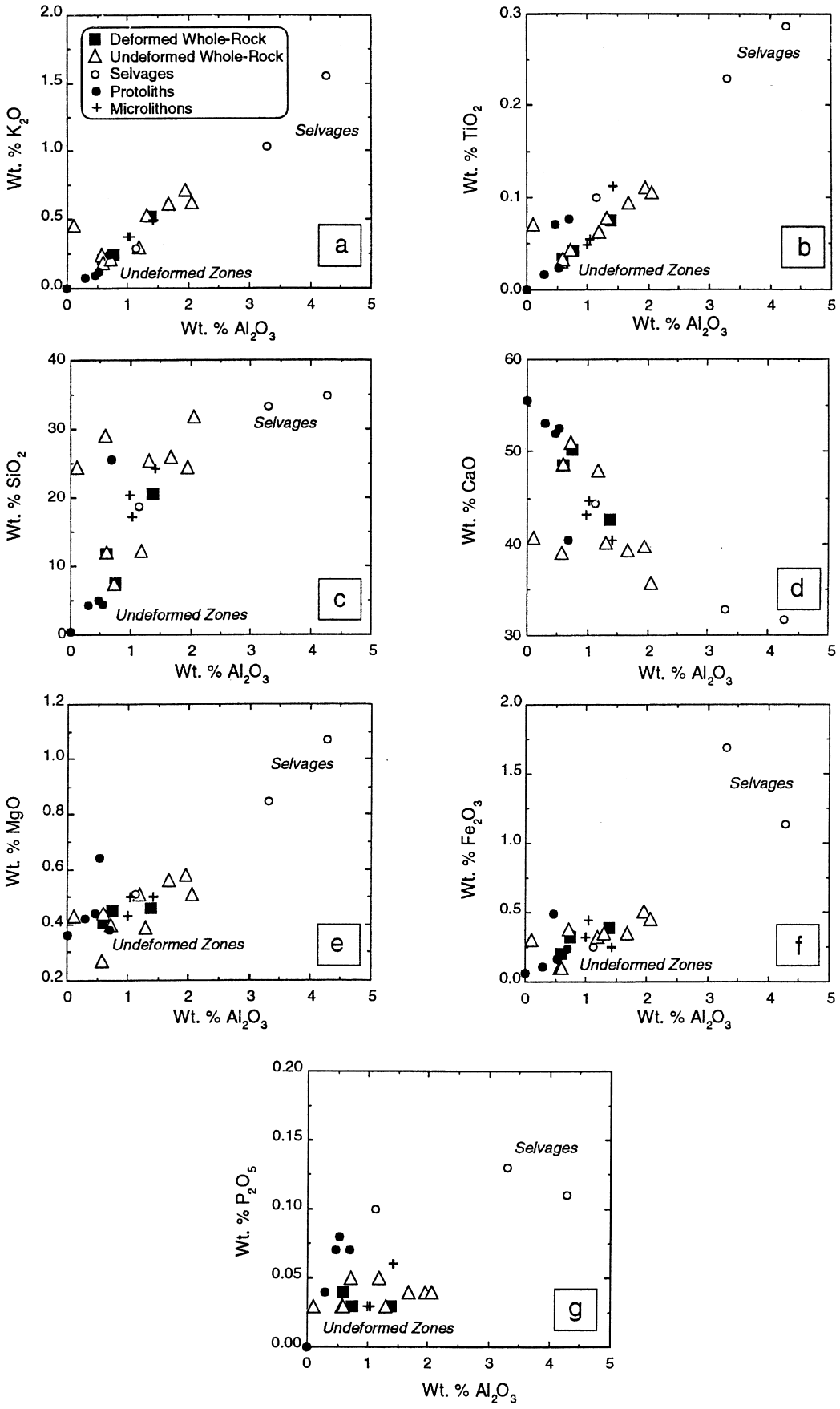

Fig. 9. (a–g) Major element whole-rock and microsampled data for samples from the lower fold. Note overlap of data for undeformed and deformed whole-rock samples, but distinct compositions among microsampled selvages and microlithons (some data for microsampled protolith samples are also provided).

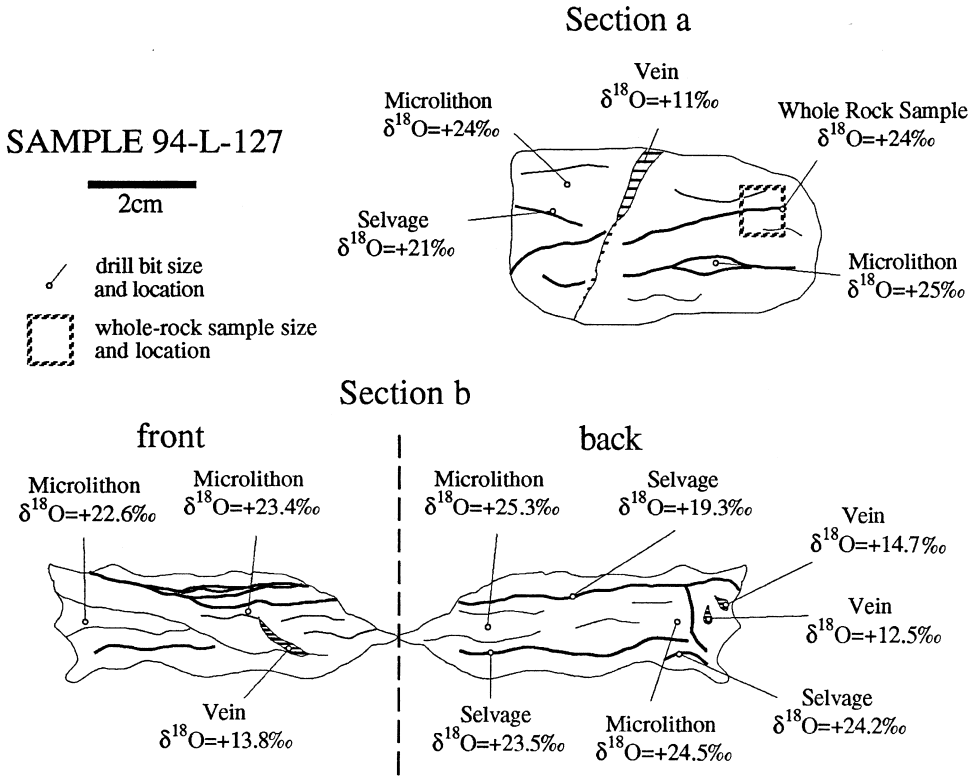

Fig. 10. Schematic of sample 94-L-127 illustrating microdrill and whole- rock O- and C-isotope values. Note differences in $\delta^{18}O$ among microdrilled selvage, microlithon and vein domains. The whole-rock sample is interpreted to be a mixture in isotopic composition of selvage and microlithon domains.

performed on calcite samples by liberation of CO_2 gas following the techniques of McCrea (1950), and using the Finnigan MAT 252 at Lehigh University. Data are presented in standard notation (in ‰), according to:

$$\delta^{18}O = 1000\left[\left(\left(^{18}O/^{16}O\right)_{Sample}/\left(^{18}O/^{16}O\right)_{Standard}\right) - 1\right] \quad (4)$$

$$\delta^{13}C = 1000\left[\left(\left(^{13}C/^{12}C\right)_{Sample}/\left(^{13}C/^{12}C\right)_{Standard}\right) - 1\right] \quad (5)$$

Oxygen and C isotope values are reported relative to Vienna Standard Mean Ocean Water (V-SMOW) and Pee Dee Belemnite (PDB), respectively. Proper standardization for the O- and C-isotope analyses was verified by analysis of various laboratory carbonate standards, including NBS-19 (calcite). Fractionation data for H_2O-calcite are from O'Neil *et al.* (1969).

For the lower fold, whole-rock $\delta^{18}O$ values for undeformed and deformed samples display statistically insignificant differences, with all whole-rock samples having values $> +20‰$ (Fig. 11a). Microdrilled samples from the lower fold, however, display large differences in $\delta^{18}O$ (Figs 10 & 11b), with the $\delta^{18}O$ of microlithons ranging from $+17.9$ to $+25.7‰$ ($n = 18$, mean $= +24.0$, $1\sigma = 1.9‰$), and selvage materials having $\delta^{18}O$ ranging from $+16.2$ to $+24.2‰$ ($n = 15$, mean $= +20.4$, $1\sigma = 2.6‰$). Eight samples microdrilled from undeformed protoliths (avoiding fossils, chert nodules, and rare discontinuous microselvages) have mean $\delta^{18}O$ of $+24.5$ ($1\sigma = 1.9‰$) similar to that of microlithons in deformed samples. Selvages tend to have higher $\delta^{13}C$ than microlithons, with some selvage values approaching $+6‰$ and all microlithon samples having values $< +2‰$ (Fig. 11b). For the middle fold, the mean $\delta^{18}O$ of the deformed whole-rock samples is somewhat lower than that of the undeformed whole-rock samples (Fig. 11a). Two undeformed whole-rock samples from the pinned hinge of the middle fold have much lower $\delta^{18}O$ near $+11‰$ (Fig. 11a).

Together, the $\delta^{18}O$ of vein calcite sampled in the field and by microdrilling from bedding-parallel veins, chert nodule overgrowths, cleavage-parallel veins, and late-stage extensional veins shows a wide range from $+7.9$ to $+26.3‰$ which encompasses the entire range in $\delta^{18}O$ observed for whole-rock and microdrilled rock samples (Fig. 11a–c). The $\delta^{13}C$ values of the veins (overall range from 0 to $+2.7‰$, excluding two samples) are more uniform than those of the deformed and undeformed rock samples (overall range, including microsampled materials, is from -2.6 to $+5.9‰$). Relatively high-$\delta^{13}C$ fibrous chert nodule overgrowths have $\delta^{18}O$ values which fall within the range for protolith samples (Fig. 11a & c). Single bedding-parallel vein complexes show variations in $\delta^{18}O$ of up to 5–10‰ among multiple generations of calcite of varying textures (e.g. fibrous or sparry, cleaved or uncleaved,

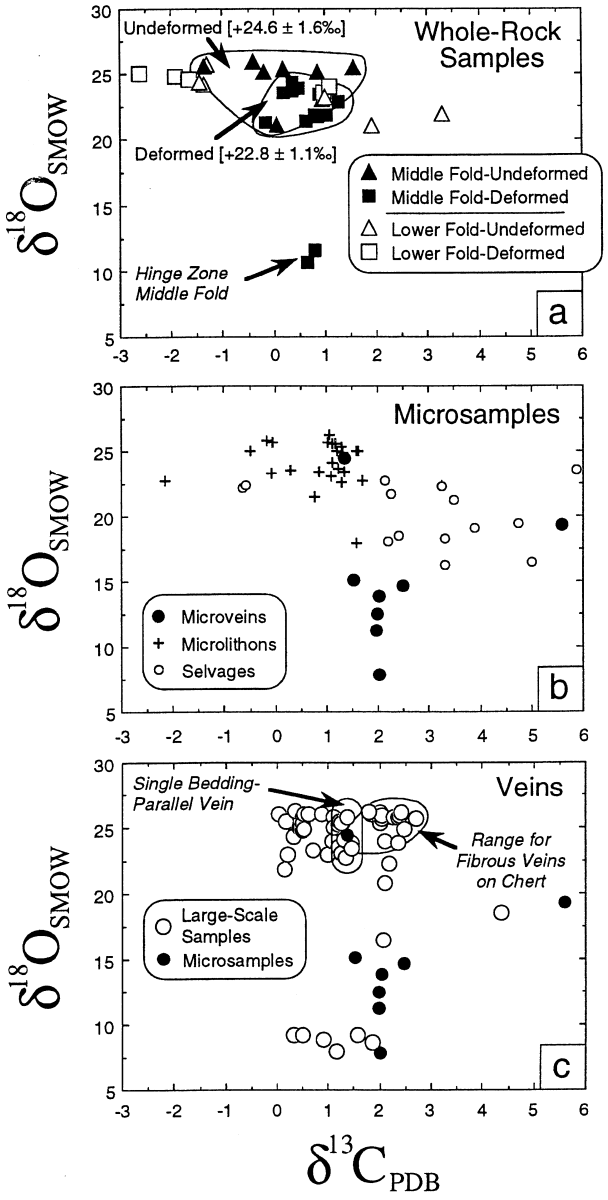

Fig. 11. Oxygen and C isotope compositions of (a) whole-rock undeformed and deformed samples from the lower and middle folds (note mean and 1σ $\delta^{18}O$ for undeformed and deformed whole-rock samples from the middle fold); (b) microsampled veins, microlithons, and selvages in five hand specimens from the lower fold; (c) microsampled veins and large-scale vein samples (collected in the field from larger vein sets). Note ranges for a single, zoned bedding-parallel vein complex in the middle fold and a zoned, fibrous veins developed on chert nodules.

Fig. 11c). Some of the larger, bedding-parallel vein complexes and other veins judged as being late-stage based on their structural position, orientation, and texture have $\delta^{18}O$ of from +5 to +10‰, with apparent leveling-off at these lower values (Fig. 11c). This range in $\delta^{18}O$ is consistent with the equilibration of the veins at temperatures of 150–250°C with H_2O-rich fluids with $\delta^{18}O$ near 0‰ (from −7.5 to +2.5‰, Bebout *et al.*, 1996).

Table 2. Major element protolith composition, mean of 4 samples with 1σ deviation. Protolith composition in wt% oxides

Oxide	Mean	One Standard Deviation
Na_2O	0.033	0.030
MgO	0.460	0.012
Al_2O_3	0.323	0.236
SiO_2	3.51	2.16
P_2O_5	0.048	0.036
K_2O	0.072	0.051
CaO	53.30	1.60
TiO_2	0.028	0.030
Fe_2O_3	0.208	0.194

Characterization of protolith samples

Representative protolith rocks were carefully sampled with regard to structural position and inspected for significant deformation textures. The four samples chosen as protoliths for this study were taken from a repeated stratigraphic layer in the hinge of the middle fold and from undeformed positions in the lower fold (Fig. 3a). Table 2 lists the average protolith compositions used in mass balance calculations with 1σ error estimates. These samples exhibit rare deformation textures such as short fibrous overgrowths and selvages in thin section. Protolith samples are devoid of macroscopic cleavage, have fairly uniform chemical composition, and record negligible finite strain including effects of compaction.

DISCUSSION

Geometry of deformation

To accurately estimate volumetric distortions, homogeneous domains of deformation must be established. Meso-scale finite strain estimates using chert nodule distributions ($2\,m^2$) suggest axial ratios of $R_{xz} = 1.9 \pm 0.2$ within the deformation zone and $R_{xz} = 1.2 \pm 0.2$ within an adjacent massive layer of the lower fold. Macro- to microscopic finite strain measurements ($1–4\,cm^2$) in samples from the same area produced equivalent results, with axial ratios of $R_{xz} = 1.8 \pm 0.3$ within shear zones and axial ratios of $R_{xz} = 1.3 \pm 0.1$ in adjacent massive layers. These results suggest that the orientation and aspect ratio of the profile plane finite strain ellipse is homogeneous over scales from a few cm to a few m (Fig. 4).

The same considerations of scale of observation and degree of homogeneity apply to the direct measurements of principal extension ($1 + e_x$). Beutner and Diegel (1985) measured host to overgrowth lengths around pyrite strain fringes in fine-grained slates and observed that the fiber-derived strains were consistent for all but the largest pyrite framboids ($> 150\,\mu m$)

and, as expected, somewhat larger than strain estimates derived by the detrital phyllosilicate method. However, Ellis (1984) reported that values of extension derived from strain fringes are widely variable and far greater than estimates determined using Fry analysis. In this study, individual overgrowths provide widely variable estimates of extension (e.g. sample 94-L-129, mean $e_x = 1.69 \pm 0.77$) in the coarse-grained carbonates of the Scott Peak Formation where large objects with overgrowths are irregularly distributed between overgrowth-rich and overgrowth-poor laminations (Figs 2 & 6). At a thin section scale (~2 cm), average principal extension values from objects with overgrowths are equivalent in multiple cleavage-parallel traverses (e.g. sample 94-L-129; mean $e_x = 0.81 \pm 0.10$), but the principal extension values are still overestimates as they ignore micro-veins and nonfibrous overgrowths (best observed in cathodoluminescence) in the matrix by evaluating mainly larger strain fringes (Fig. 6a & b). Homogeneous determinations of principal extensions can be established by determining principal extension in small overlapping domains (e.g. sample 94-L-129, mean $e_x = 0.26 \pm 0.01$ (1σ), Fig. 7c). A window length of 8 mm (2–4 times the average strain fringe size), was used in this study.

At a scale of a few cm, both relative axial ratios (R_{xz}, R_{xy}) and principal extensions ($1 + e_x$) have been determined within homogeneous domains and used to calculate $1 + e_y$, $1 + e_z$, and ΔV. A plot of principal extension values vs amount of strain ($\bar{\varepsilon}_s$; Fig. 12) shows that, at low strains ($\bar{\varepsilon}_s < 0.15$), extension in the X direction is nearly balanced by shortening in the Z direction with little change in Y or volumetric dilation (Fig. 7). At progressively higher strains ($\bar{\varepsilon}_s > 0.15$ up to 0.53), lengthening in the X direction continues almost linearly but is accompanied by significant shortening in both the Z and Y directions (Fig. 12). The onset of shortening in the Y direction results in a transition from oblate to prolate strains (Fig. 5). At low values of strain, dilatancies of from −2% to −12% were calculated. A higher strains, with both Y and Z shortening, volume losses of from −20% to −50% were determined (Fig. 7). Cleavage intensity also correlates well with the amount of strain and amount of volume loss experienced, with strongly- to very strongly-cleaved rocks having lost the most material at the thin section scale, and rocks which have no cleavage to very weak cleavage showing little or no volume loss (Fig. 7).

The calculated shortening in Y is suspected to be local at the duplex as it is not observed elsewhere where we have worked in the Lost River Range (Fisher and Anastasio, 1994; Anastasio *et al.*, 1997). There is a noticeable absence of microscopic textures indicative of shortening or flow parallel to Y in the samples examined; however, the Doublespring duplex exposure is somewhat two-dimensional, making larger-scale, strike-parallel observations difficult. Straight, fibrous overgrowths parallel to dip of cleavage (X) are ubiquitous and overgrowths parallel to Y were not found. A possible explanation for local shortening along strike is the northward convergence of fold axes of the lower and middle folds likely resulting from differing thrusting directions during duplex development.

As is sometimes overlooked, volume strain assessments are dependent upon the scale of observation. As indicated by Fig. 13, evidence of volume gains and losses coexists at a thin section scale, with fibrous overgrowths and micro-veins reflecting local gains and truncated fossils and sutured grain boundaries recording local losses. At a millimeter scale, transgranular cleavage surfaces record volume losses; however, cleavage is only locally developed within the duplex. Calcite overgrowths on chert nodules and layer-paral-

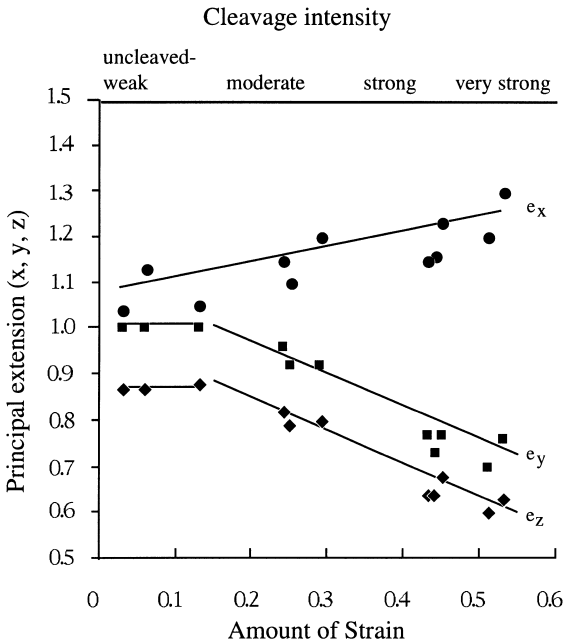

Fig. 12. Plot of principal extensions (e_x,e_y,e_z) vs $\bar{\varepsilon}_s$ and cleavage intensity. e_x increases almost linearly, whereas, at low strains, shortening occurs only in the Z direction and at higher strains, shortening occurs in the Y direction as well.

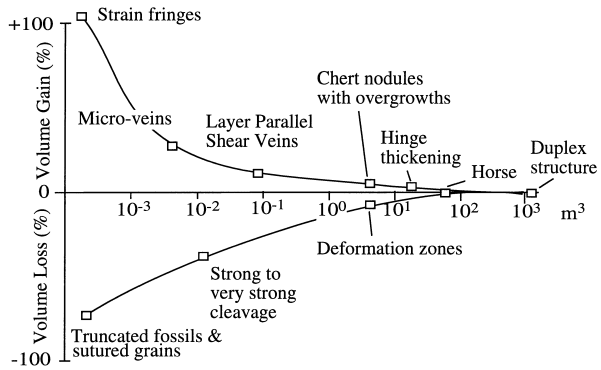

Fig. 13. Schematic illustrating variability of volume strains according to scale of observation at Doublespring duplex. Curve fit through scale-independent assessments of dilatency. At the outcrop scale, loss due to cleavage formation is negligible.

lel shear veins exhibit evidence of volume gains in areas over scales of up to a few meters. Larger-scale mass redistribution of material along layers from the limb towards the hinge of the middle fold created thickening and thinning over tens of meters. The heterogeneity of volume strain increases as the scale scale of observation decreases within the Doublespring duplex. For example, in the middle fold of the duplex, application of maximum volume loss at a thin section scale to cleaved rocks of the middle fold (−50% in sample IH92-001) plus an estimate of volume gains from veins across the entire middle fold suggests that actual mesoscopic volume loss (hundreds of m^3–1 km^3) is quite small, ~3% (Fig. 14).

Scale of sampling and geochemical analysis

The scale of sampling is equally important when considering the geochemical data. In a pilot geochemical study examining differences between undeformed and deformed whole-rock samples (sampling scales of approximately 10–15 cm^3) from the middle fold shear zone in the Doublespring duplex, volume loss estimates of up to 90% were made assuming only passive concentration occurred and using the dramatic Al and Ti element enrichments relative to the inferred protolith (Hedlund *et al.*, 1993). Hedlund *et al.* (1993) noted, however, that such large volume losses are incompatible with the cylindrical, parallel fold geometries. As in the earlier study, XRF and stable isotope analyses of whole rock samples in the present study (from the lower fold, at scales of ~4–7 cm^3) produced results which do injustice to the scale and degree of chemical heterogeneity and their implications for the processes of cleavage formation (Figs 8, 10 & 11a). Microdrilling at scales of a few mm^3 to 1 cm^3 demonstrates more clearly the distinctive isotopic and major element compositions of selvage materials, microlithons, protoliths, and veins (Figs 9, 10 & 11b). The utility of the whole-rock geochemical approach towards assessing volume strain and metasomatism is diminished by the mixing of selvage and microlithon compositions. The data for microdrilled protolith, microlithon, and selvage materials better allow geochemical comparisons of the variably cleaved rocks with the protolith, and therefore, better afford assessments of the mass transfer processes operating within and among the textural domains.

Mass balance and protolith composition

Geochemical approaches to estimating volume strain and mass transfer traditionally mass-balance deformed rock compositions relative to an inferred protolith or use a reference species assumed to be immobile (normally Al or Ti, e.g. Erslev and Mann, 1984; Ague,

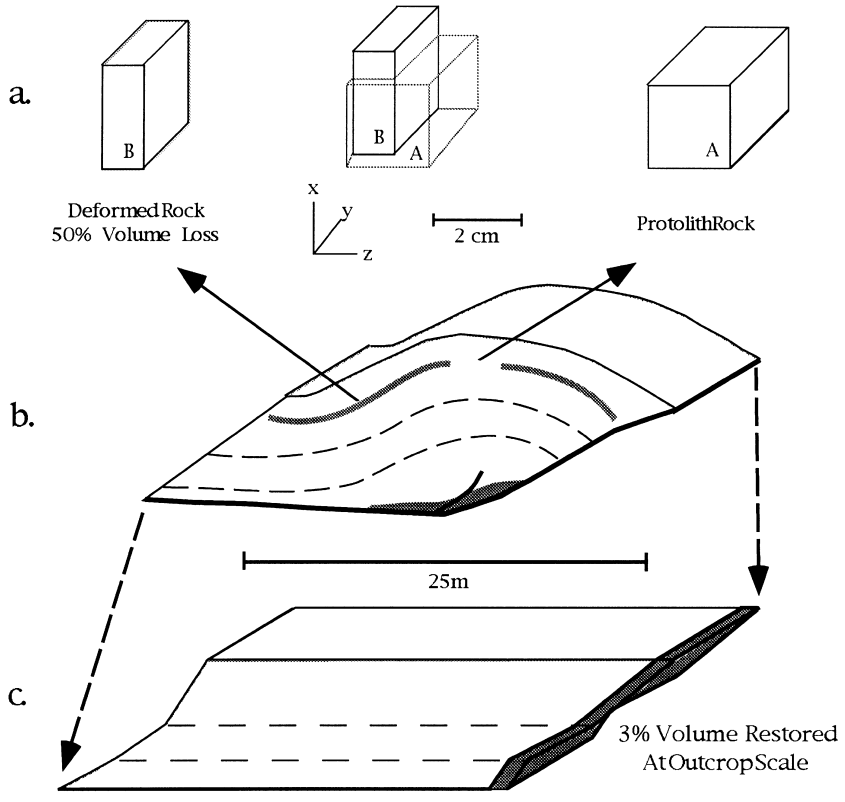

Fig. 14. Schematic illustration of dilatency partitioning in thin deformation zones in Doublesprings duplex horse. At a small-scale (~3–4 cm^3), maximum volume losses of ~50% were estimated. Applying this value with consideration to strain localization and measurable material additions from layer-parallel veins and overgrowths, an estimated < 3% of volume loss for the entire outcrop (from 100 m^3 to 1 km^3) is derived.

1991; Goldstein, 1996). In this study, we used a locally determined protolith that can be directly related lithologically and spatially to the deformed equivalents, exploiting the well-known structure and kinematics of the Doublespring duplex. In this section, we use comparisons of enrichments of various elements in variably deformed samples relative to inferred protolith compositions to deduce the extent to which enrichments in each of the elements can be explained by passive concentration or, alternatively, must be explained by metasomatic additions. The samples for these mass-balance calculations are selvage-microlithon pairs from two strongly cleaved samples (94-L-124 and 94-L-127) and a less extensively developed selvage from a less deformed sample (94-L-3).

Textural, mineralogical and geochemical evidence suggests that Ca depletion accompanying calcite dissolution dominates the volume losses. As is shown in Fig. 15, greater enrichments of certain major elements (points that lie above the line indicating a sample to average protolith ratio of 1) occur in the selvage samples showing greater Ca depletion (up to ~40% loss of Ca in selvage samples 94-L-124B and 94-L-127B). For the two selvage–microlithon pairs, selvage samples are significantly more enriched in most elements, particularly K, Al, Si, Ti and Fe, relative to microlithons from the same samples (94-L-124A and 94-L-127A). The microlithons from the two more deformed samples are extremely similar in composition to the selvage in the less deformed sample (sample 94-L-3A; see comparisons in Fig. 15a & b). The two microlithons and the selvage in sample 94-L-3 show similar extents of Ca depletion (< 20%) lower than that for the two selvage samples (~40%).

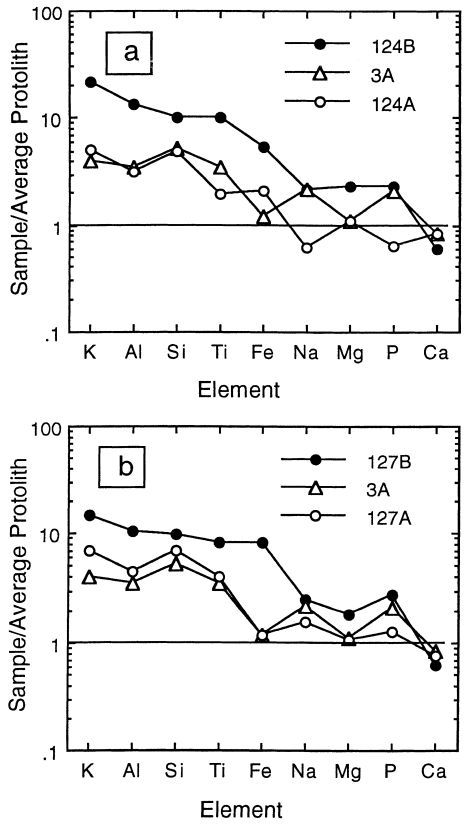

Fig. 15. Plot of element enrichment or depletion of major elements for (a) sample 94-L-127, and (b) 94-L-124, both strongly cleaved, normalized to the protolith composition. Values > 1 indicate enrichment, and values < 1 indicate depletion (note the logarithmic scale), relative to the concentrations of each element in the protolith. Note the similarity in composition of microlithons in each sample (indicated as 124A and 127A; 124B and 127B are selvage compositions in the same two samples) to the selvage in the less deformed sample 94-L-3A.

Previous models of cleavage formation in carbonate rocks (e.g. Alvarez *et al.*, 1978; Engelder and Marshak, 1985) have argued that passive concentration is the primary mechanism of selvage development. An analysis of the data in Fig. 15 demonstrates that passive concentration (i.e. as related simply to varying degrees of calcite removal by dissolution) can better account for the enrichments of some elements than for others. Using the amount of Ca depletion in selvages relative to the average protolith as a reference, we have estimated the maximum percentages of enrichment of each element attributable to simple passive concentration (Table 3). The enrichments of some elements, specifically Na, Mg and P are more consistent with enrichment by passive concentration (i.e. showing enrichment to approximately double the protolith concentrations consistent with the losses of up to ~40% Ca as calcite). The simple passive concentration model can, in general (excluding P), explain higher percentages of the element enrichment in the less cleaved sample 94-L-3A than in the more cleaved microsamples (94-L-124B and 94-L-127B). Table 3 demonstrates that the enrichments in K, Al, Si, Ti and possibly Fe are particularly unsuccessfully explained by passive concentration alone (that mechanism accounts for < 20% of the enrichment in each of these elements). In selvage samples (94-L-124B, 94-L-127B), each of these elements is enriched to > 5 times its concentration in protoliths and four of the elements (K, Al, Si and Ti) are enriched to > 10 times the protolith concentrations. Therefore, significant metasomatic enrichments of these elements are required (Fig. 15).

Table 3. Maximum percentages of element enrichment attributable to passive concentration. See text for discussion

Element	94-L-127B very strongly cleaved	94-L-124B strongly cleaved	94-L-3A weakly cleaved
Na	48	53	74
Mg	43	33	96
Al	11	9	42
Si	19	18	32
P	60	106	22
K	8	5	35
Ti	16	12	49
Fe	15	22	134

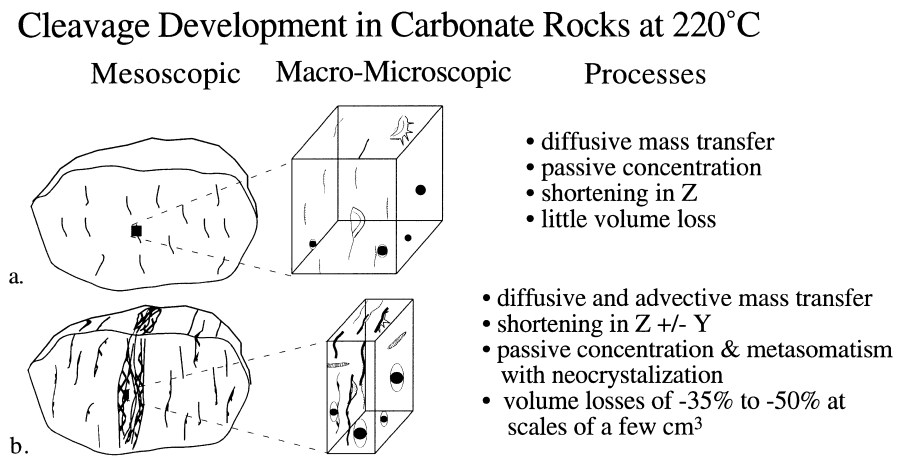

Fig. 16. Summary of conceptual model of cleavage development in low-grade carbonate rocks. (a) Nascent selvages characteristic of weakly-cleaved samples, (b) well-developed selvages characteristic of strongly cleaved samples.

Open and closed system behavior and mechanisms of cleavage development

The major element, trace element, and stable isotope data all require some open-system behavior during the development of cleavage in the Doublespring duplex samples. Microsample O-isotope results clearly differentiate among protolith, microlithon, selvage domains, and vein materials (Fig. 10). The shifts in $\delta^{18}O$ of up to ~20‰ cannot be explained by closed-system behavior but are consistent with the varying infiltration of the rocks, along deformation zones and fractures, by externally-derived fluids having likely experienced a wide range of upstream fluid–rock isotopic exchange histories. Based on data from the Doublespring locality and several other localities in the Lost River and Beaverhead Ranges (Idaho and Montana), we inferred that the shifts and a regional leveling-off of the calcite $\delta^{18}O$ values for late-stage veins and some deformed rocks in the +5 to +10‰ range are consistent with the infiltration of the rocks by H_2O-rich fluids with $\delta^{18}O$ initially near 0‰ (from −7.5 to 2.5‰) at temperatures of 150°–250°C inferred for the deformation and vein formation (Bebout *et al.*, 1996). The leveling-off and range of late-stage vein $\delta^{18}O$ values was interpreted to reflect penetration of the evolving thrust belt by surficial fluids in a hydrologic regime with a strong seawater influence (likely nearshore meteoric water), consistent with the paleogeographic reconstructions for the area indicating the presence of an intracontinental seaway (the Western Interior Seaway; see data for analogous modern setting in Kendall *et al.*, 1995). The somewhat higher $\delta^{13}C$ values of fibrous chert overgrowths were interpreted to reflect relatively closed-system C-isotope partitioning during early-stage local-scale diffusional mass transfer (Bebout *et al.*, 1996). The protolith-like $\delta^{18}O$ values of the chert overgrowths are thought to reflect extensive buffering of the $\delta^{18}O$ of the infiltrating fluid by the rocks. Later-stage fluid flow was dominantly discontinuity-based (i.e. along cleavage selvages, faults, and fracture networks), and fluids infiltrating along discontinuities better retained the O-isotope compositions of their sources (i.e. were less altered than the early fluids in their $\delta^{18}O$ by upstream fluid-rock exchange). Differences in $\delta^{18}O$ among protolith, microlithon, and selvage materials suggest that strain enhances the degree of infiltration by fluids and thereby facilitates cleavage development. Some major element enrichments in selvage material are more consistent with simple passive concentration; however, enrichments in K, Al, Si and Ti (and possibly Fe) appear to require significant enrichment of these elements as the result of fluid-rock interactions. The infiltrating fluids would have also provided the mechanism for the significant localized redistribution of Ca evident in many of the deformed samples.

The geochemical data are consistent with the progressive development of cleavage through a combination of passive concentration and metasomatism. The varying degrees of element enrichment, corresponding to varying extents of progressive deformation in microlithons and selvages and among weakly to intensely cleaved whole-rock samples, reflect a continuum in the extents of coupled deformation, fluid-rock interaction, and related metasomatism. Initially, rare detrital clay minerals (< 1 wt% illite) and oxides (< 15 wt%) present within the protolith matrix localized grain sutures. Coincident with shortening in Z, an oblate fabric developed under closed-system conditions. Fibrous overgrowths, which were formed by diffusional mass transfer, have $\delta^{18}O$ and cathodoluminescence signatures similar to those of protoliths, whereas well-developed selvages and later-stage veins have signatures attributable to exchange with externally-derived fluids. This interpretation suggests that, as diffusion mass transfer continued to form transgranular sutures, fluid infiltration in nascent selvages became enhanced, making advection possible and allowing increased element exchange and addition (Fig. 16). Microlithons with chemical compositions in-

termediate to those of protoliths and selvages represent varying intermediate stages of this process. Microlithons contain microselvages visible only at high magnification using the SEM. Selvages began to act as discrete and preferential flow paths for migrating fluids capable of introducing externally-derived materials, in this case, K, Al, Si and Ti to crystallize illite, kaolinite, quartz, and anatase. Geometric and geochemical strain softening occurred with calcite loss and clay precipitation, further accelerating the diffusional mass transfer processes (cf. Marshak and Engelder, 1985).

CONCLUSIONS

Utilizing integrated structural and geochemical analysis, the results of this study provide new information regarding the mechanisms of cleavage development in carbonate rocks. It has been shown that observations and measurements of volume strain require careful attention to scale. The rocks from Doublespring duplex which illustrate significant volume losses in strongly cleaved rocks at a scale of a few cm^3, but only a small volume loss of $< 3\%$ over the entire outcrop.

Mass redistribution related to cleavage formation at Doublespring duplex was heterogeneous over seven orders of magnitude. At a scale of a few cm, in homogeneous domains, shortening occurred at low strains parallel to Z, then along both Y and Z at higher strains as cleavage developed. Finite strain calculations suggest that strong cleavage was associated with volume losses of up to 50% over volumes of 3–4 cm^3. Due to the varying scales of sampling between the approaches, reconciliation of the geometrical and geochemical volume strain estimates is not expected. At scales of homogeneous finite strain (a few cm^3), mixtures of selvage and microlithon domains obscure the geochemical signatures of volume loss.

Geochemical analysis suggests that cleavage selvage development is facilitated by a depletion of calcium (by loss of calcite from local domains), combined with external additions of K, Al, Si, Ti and possibly Fe. Shifts in O-isotope compositions indicate open-system behavior during cleavage formation. Cleavage formation in the carbonates at Doublespring duplex developed by a combination of passive concentration involving pressure solution, which localized selvages and accommodated volumetric dilations, and metasomatic additions which increased with strain and enhanced neo-crystallization. As strain increased, selvages coalesced, becoming longer, thicker, and more discrete, thus channeling fluid flow and enhancing metasomatism. The metasomatism led to the neo-crystallization of selvage mineral phases illite, kaolinite, quartz and anatase.

Acknowledgements—Financial support for this project, Davidson's M.S. degree, and Holl's postdoctoral appointment was provided by NSF grant EAR-9405626 awarded to Anastasio and Bebout. Davidson acknowledges a grant from the Geological Society of America which supported M.S. research and funding from NSF grant EAR-9100982 (a consortial REU site project) which supported preliminary strain analysis completed as a B.S. Honors thesis. Funds from NSF grant EAR-9017334 awarded to Anastasio and a Lehigh University Faculty Research Grant awarded to Bebout supported the preliminary geochemical analysis completed by Hedlund. Comments on the manuscript by D. R. Gray and an anonymous reviewer and the editorial efforts of R. J. Lisle were much appreciated.

REFERENCES

Ague, J. (1991) Evidence for major mass transfer and volume strain during regional metamorphism of pelites. *Geology* **9,** 855–858.

Ague, J. (1994) Mass transfer during Barrovian metamorphism of pelites, south-central Connecticut. I: Evidence for changes in composition and volume. *American Journal of Science* **294,** 989–1057.

Alvarez, W., Engelder, T. and Lowrie, W. (1976) Formation of spaced cleavage and folds in brittle limestones by dissolution. *Geology* **4,** 698–701.

Alvarez, W., Engelder, T. and Geiser, P. A. (1978) Classification of solution cleavage in pelagic limestones. *Geology* **6,** 263–266.

Anastasio, D. J., Fisher, D. M., Messina, T. H. and Holl, J. E. (1997) Kinematics of décollement folding: Lost River Range, Idaho. *Journal of Structural Geology* **19,** 355–368.

Bailey, C. M., Simpson, C. and De Paor, D. G. (1994) Volume loss and tectonic flattening strain in granitic mylonites from the Blue Ridge Province, Central Appalachians. *Journal Structural Geology* **16,** 1403–1416.

Bebout, G. E., Holl, J. E., Anastasio, D. J. and Davidson, S. G. (1996) Characterizing Late Cretaceous to Eocene regional crustal fluid infiltration in central Idaho. *Geological Society of America, Abstracts with Programs* **28,** A254.

Beutner, E. C. and Charles, E. G. (1985) Large volume-loss during cleavage formation, Hamburg, sequence, Pennsylvania. *Geology* **13,** 803–805.

Beutner, E. C. and Diegel, F. A. (1985) Determination of fold kinematics from syntectonic fibers in pressure shadows, Martinsburg slate, New Jersey. *American Journal of Science* **285,** 16–50.

Davidson, S. G. (1996) Volume loss and metasomatism during cleavage formation in carbonate rocks. M.S. thesis. Lehigh University.

Davidson, S. G., Anastasio, D. J. and Bebout, G. E. (1996) Passive concentration and metasomatism during cleavage development in carbonate rocks, Lost River Range, Idaho. *Geological Society of America, Abstracts with Programs* **28,** A246.

De Paor, D. G., Simpson, C., Bailey, C. M., McCaffrey, K. J. W., Beam, E., Gower, R. J. W. and Aziz, G. (1991) The role of solution in the formation of boudinage and transverse veins in carbonate rocks at Rheems, Pennsylvania. *Bulletin of the Geological Society of America* **103,** 1552–1563.

Drever, J. I. (1973) The preparation of oriented clay mineral specimens for X-ray diffraction analysis by a filter-membrane peel technique. *American Mineralogy* **58,** 553–554.

Ellis, M. A. (1984) Strain measures derived from grain shape-fabrics and syntectonic crystal fibers: A comparison. *Geological Society of America, Abstracts with Programs* **16,** 501.

Engelder, T. and Marshak, S. (1985) Disjunctive cleavage formed at shallow depths in sedimentary rocks. *Journal of Structural Geology* **7,** 327–343.

Erslev, E. A. and Mann, C. (1984) Pressure solution shortening in the Martinsburg Slate, New Jersey. *Proceedings of the Pennsylvania Academy of Science*, **58,** 84–88.

Erslev, E. A. (1988) Normalized center-to-center strain analysis of packed aggregates. *Journal of Structural Geology* **10,** 201–209.

Erslev, E. A. and Ward, D. J. (1994) Non-volatile element and volume flux in coalesced slaty cleavage. *Journal of Structural Geology* **16,** 531–553.

Fisher, D. M. and Anastasio, D. J. (1994) Kinematic analysis of a large-scale leading edge fold, Lost River Range, Idaho, U.S.A. *Journal of Structural Geology* **16,** 571–584.

Geiser, P. A. (1974) Cleavage in some sedimentary rocks of the central Valley and Ridge Province, Maryland. *Bulletin of the Geological Society of America* **85,** 1399–1412.

Goldstein, A., Pickens, J., Klepeis, K. and Linn, F. (1995) Finite strain heterogeneity and volume loss in slates of the Taconic Allochthon, Vermont, U.S.A. *Journal of Structural Geology* **17,** 1207–1216.

Gray, D. R. (1978) Cleavages in deformed psammitic rocks from southeastern Australia; Their nature and origin. *Bulletin of the Geological Society of America* **89,** 577–590.

Gray, D. R., Gregory, R. T. and Durney, D. W. (1991) Rock-buffered fluid-rock interaction in deformed quartz-rich turbiditic sequences, eastern Australia. *Journal of Geophysical Research* **96,** 19681–19704.

Groshong, R. H. (1975) Strain, fractures, and pressure solution in natural single layer folds. *Bulletin of the Geological Society of America* **86,** 1363–1376.

Hedlund, C. A., Bebout, G. E. and Anastasio, D. J. (1993) Mass transfer during cleavage formation in carbonate shear zones, Doublespring Duplex, Idaho. *EOS Transactions, American Geophysical Union* **74,** 302.

Hedlund, C. A., Anastasio, D. J. and Fisher, D. M. (1994) Kinematics of fault-related folding in a duplex, Lost River Range, Idaho, U.S.A. *Journal of Structural Geology* **16,** 571–584.

Hein, J. R., Scholl, D. W. and Gutmacher, C. E. (1975) Neogene clay minerals of the far NW-Pacific and southern Bering Sea: Sedimentation and diagenesis. *Proceedings of the International Clay Conference*, pp. 71–92.

Hossack, J. R. (1968) Pebble deformation and thrusting in the Bygdin area (S. Norway). *Tectonophysics* **5,** 315–339.

Kendall, C., Sklash, M. G. and Bullen, T. D. (1995) Isotope tracers of water and solute sources in catchments. In *Solute Modelling in Catchment Systems*, ed. S. T. Trudgill, pp. 261–303. John Wiley and Sons, New York.

Kerrich, R. (1986) Fluid infiltration into fault zones: chemical, isotopic, and mechanical effects. *Pure and Applied Geophysics* **124,** 225–268.

Kirschner, D. L., Teyssier, C., Gregory, R. T. and Sharp, Z. D. (1995) Effect of deformation on oxygen isotope exchange in the Heavitree Quartzite, Ruby Gap duplex, central Australia. *Journal of Structural Geology* **17,** 1407–1423.

Lee, J. H., Peacor, D. R., Lewis, D. D. and Winstch, R. P. (1986) Evidence for syntectonic crystallization for the mudstone to slate transition at Lehigh Gap, Pennsylvania. *Journal of Structural Geology* **8,** 767–780.

Marshak, S. and Engelder, T. (1985) Development of cleavage in limestones of a fold-thrust belt in New York. *Journal of Structural Geology* **7,** 345–359.

McCrea, J. M. (1950) The isotopic chemistry of carbonates and a paleotemperature scale. *Journal of Chemical Physics* **18,** 849–857.

Nadai, A. (1963) *Theory of flow and fracture of solids*. McGraw-Hill, New York.

Nickelsen, R. P. (1972) Attributes of rock cleavage in some mudstones and limestones of the Valley and Ridge Province, Pennsylvania. *Proceedings of the Pennsylvania Academy of Science*, **46,** 107–112.

O'Neil, J. R., Clayton, R. N. and Mayeda, T. K. (1969) Oxygen isotope fractionation in divalent metal carbonates. *Journal of Chemical Physics* **51,** 5547–5558.

Ramsay, J. G. and Huber, M. I. (1983) *The Techniques of Modern Structural Geology, V.1: Strain Analysis*. Academic Press, London.

Ramsay, J. G. and Wood, D. S. (1973) The geometric effects of volume change during deformation processes. *Tectonophysics* **16,** 263–277.

Rye, D. M. and Bradbury, H. J. (1988) Fluid flow in the crust: An example from a Pyrenean thrust ramp. *American Journal of Science* **288,** 197–235.

Schwietzer, J. and Simpson, C. (1986) Cleavage development in dolomite of the Elbrook Formation, southwest Virginia. *Bulletin of the Geological Society of America* **97,** 778–786.

Silverberg, D. S. (1990) The tectonic evolution of the Pioneer metamorphic core complex, south-central Idaho. Ph.D. dissertation, Massachusetts Institute of Technology.

Srivastava, H. B., Hudleston, P. and Earley III, D. (1995) Strain and possible volume loss in a high grade ductile shear zone. *Journal of Structural Geology* **17,** 1217–1231.

Wintsch, R. P., Kvale, C. M. and Kisch, H. J. (1991) Open-system, constant-volume development of slaty cleavage, and strain induced replacement reactions in the Martinsburg Formation, Lehigh Gap, Pennsylvania. *Geological Society of America Bulletin* **103,** 916–927.

Wright, T. O. and Henderson, J. R. (1992) Volume loss during cleavage formation in the Meguma Group, Nova Scotia, Canada. *Journal of Structural Geology* **14,** 281–290.